HAL open science

Quantitative evaluation of phase retrieval algorithms in propagation based phase tomography

M. Langer, P. Cloetens, J. P. Guigay, S. Valton, F. Peyrin

To cite this version:

M. Langer, P. Cloetens, J. P. Guigay, S. Valton, F. Peyrin. Quantitative evaluation of phase retrieval algorithms in propagation based phase tomography. 4th IEEE International Symposium on Biomedical Imaging: Macro To Nano, Apr 2007, Arlington, United States. pp.552-555, 10.1109/ISBI.2007.356911 . hal-01825262

HAL Id: hal-01825262

https://hal.science/hal-01825262v1

Submitted on 27 Jun 2022

HAL is a multi-disciplinary open access archive for the deposit and dissemination of scientific research documents, whether they are published or not. The documents may come from teaching and research institutions in France or abroad, or from public or private research centers.

L'archive ouverte pluridisciplinaire **HAL**, est destinée au dépôt et à la diffusion de documents scientifiques de niveau recherche, publiés ou non, émanant des établissements d'enseignement et de recherche français ou étrangers, des laboratoires publics ou privés.

Distributed under a Creative Commons Attribution - NonCommercial 4.0 International License

QUANTITATIVE EVALUATION OF PHASE RETRIEVAL ALGORITHMS IN PROPAGATION BASED PHASE TOMOGRAPHY

M. Langer(1,2), P. Cloetens(1), J.P. Guigay(1), S. Valton(2), F. Peyrin(1,2)

(1) ESRF, BP220, 38043 Grenoble Cedex, France
(2) CREATIS, UMR CNRS 5515, U630 INSERM, Lyon, France

ABSTRACT

Phase contrast provides new possibilities in X-ray imaging, offering up to 1000 times higher sensitivity than standard absorption contrast. In propagation based phase contrast imaging, a quantitative relationship exists between intensity in the image plane and the phase shift induced by the object. Inversion of this relationship is called phase retrieval. Used as input to a 3D tomographic reconstruction algorithm this gives a reconstruction of the refractive index. Several methods for phase retrieval have been described, but few quantitative studies have been performed. In this paper we describe three phase retrieval methods, respectively based on the Transport of Intensity Equation (TIE), Contrast Transfer Function (CTF) and a Mixed approach recently developed at the ESRF. The methods are evaluated using simulated and experimental data in the case of mixed absorption and phase objects. Using the TIE on simulated data we obtain a reconstruction with a mean error of 10 %, but fail to achieve a qualitatively acceptable reconstruction of experimental data. The CTF approach yields qualitative reconstructions both using simulated and experimental data. Using the Mixed approach, we obtain reconstructions with close correspondence to expected values with an average errors of 3.8 % for the simulated and 5.9 % for the experimental data.

Index terms Microscopy, Simulation, Synchrotron Radiation, Tomography, X-ray imaging

1. INTRODUCTION

Micro-CT (computed tomography) imaging systems are increasingly used for biomedical and small animal imaging. The high useful flux generated by synchrotron sources makes them very attractive for micro-CT, enabling 3D imaging at sub-micrometer resolution while maintaining high signal to noise ratio. Micro-CT images are obtained by exploiting the attenuation property of x-ray interaction with matter. The coherency property of synchrotron radiation (SR) x-rays however enables another imaging mode based on phase contrast. This modality allows imaging of low-Z materials or interfaces between materials with similar attenuation properties, offering up to 1000 times higher sensitivity [1] and is particularly attractive for imaging biological soft tissues. The coherence of beams generated by third generation synchrotron sources allows a particularly simple mode of phase contrast imaging based on free space propagation that is analogous to the defocusing technique in electron microscopy.

This technique can be coupled to micro-CT by acquiring tomographic scans at several sample to detector distances (Fig. 1). The method is called holotomography [2] and the inversion process works in two steps: in the first step, called phase retrieval, the phase shift induced by the sample is calculated for each projection angle. This is then used as input to a 3D tomographic reconstruction algorithm, which yields the refractive index distribution of the sample, which is related to the electron density.

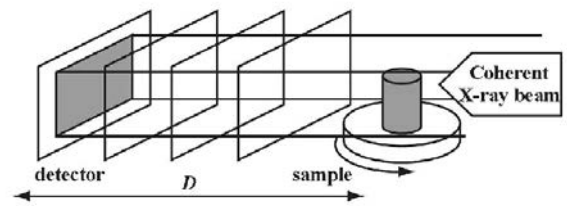

Fig. 1. Schematic view of the experimental setup used in propagation based imaging. The images recorded at different distances are used to retrieve the phase of the wave exiting the sample. These phase maps allow reconstructing the 3D refractive index decrement distribution in the sample.

The phase retrieval step is crucial for the quality of the final 3D reconstructed image. Methods well adapted to objects with "weak" absorption properties have been proposed and successfully applied to several problems in materials and life sciences, where it is crucial to enhance the sensitivity or reduce the dose compared to absorption CT [3].

In this work we address the problem of quantitative phase retrieval in mixed absorption/phase objects. Extracting quantitative information from images containing both phase and absorption contrast is still a challenging issue. Although several theoretical approaches have been proposed, there are few works addressing the quantitative evaluation of such methods [4]. We consider three methods based on the Transport of Intensity Equation (TIE) [5], Contrast Transfer Functions (CTF) [6] and a mixed approach between the two recently developed at the ESRF [7]. We evaluate them using both simulated and real data using a constructed phantom.

2. IMAGE FORMATION

The image formation process in propagation based imaging is well described in the framework of Fourier optics. By using coherent X-rays, the contrast in the image formed on the detector is not only due to absorption but also to the phase shift induced by the object. In the following we assume that we work with monochromatic x-rays with wavelength . Let $n(x,y,z) = (1-\eta(x,y,z)) + i\beta(x,y,z)$ be the 3D complex refractive index distribution in the object. The image formation process may be modelled as a function of the transmittance $T(\mathbf{x}) = a(\mathbf{x})\exp[i\varphi(\mathbf{x})]$ where $a(\mathbf{x}) = \exp[-\frac{2\pi}{\lambda}\int\beta(x,y,z)\mathrm{d}z]$ and $\varphi(\mathbf{x}) = \varphi_0 - \frac{2\pi}{\lambda}\int\eta(x,y,z)\,\mathrm{d}z$ and $\mathbf{x} = (x,y)$ are the coordinates in the image plane. The image formed on the detector, when the beam is allowed to propagate after interaction with the object by moving the detector away a distance D, is

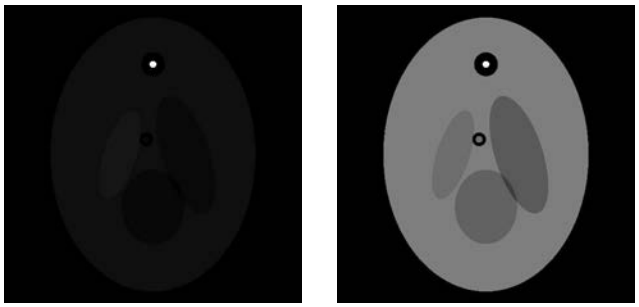

(a) Linear attenuation coefficient (b) Refractive index decrement

Fig. 2. Central slice of the phantom used in the simulations. It is based on the 3D Shepp-Logan phantom, modified to the physical values of the materials used in the constructed phantom below. Areas of zeros were also added around the parts corresponding to polymer and aluminium to closer emulate the qualitative behaviour of the constructed phantom.

a diffraction pattern. This is formed by the interference between the part of the wave that interacts with the sample and the part that goes through unaffected. The Fourier transform of the intensity recorded by the detector $\tilde{I}_D(\mathbf{f})$, where $\mathbf{f} = (f_x, f_y)$ are the spatial frequency coordinates, can be described as [6]

$$I_D(\mathbf{f}) = \int T\left(\mathbf{x} - \frac{\lambda D \mathbf{f}}{2}\right) T^*\left(\mathbf{x} + \frac{\lambda D \mathbf{f}}{2}\right) \exp(-i2\pi \mathbf{x} \cdot \mathbf{f}) \mathrm{d}\mathbf{x} \tag{1}$$

where $\mathbf{x} \cdot \mathbf{f}$ denotes scalar product between vectors $\mathbf{x}$ and $\mathbf{f}$.

If $D = 0$ Eq. 1 reduces to the standard absorption law used in conventional X-ray CT. If $D > 0$ the intensity is dependent on both the absorption and phase shift due to the object. Since the phase shift is directly proportional to the projection of the 3D refractive index decrement $\eta(x, y, z)$, if the phase shift can be calculated in each projection, this quantity can be reconstructed using standard 3D tomographic reconstruction algorithms.

3. PHASE RETRIEVAL

Inferring the phase of the wavefront from recorded intensity images is termed phase retireval. Eq. 1 is non-linear however, and no direct way to invert this relationship is known. The three methods we compare here are all based on linearizing some aspect of Eq. 1 to obtain an expression that can be solved for the phase and is applicable in practice.

3.1. Transport of Intensity Equation (TIE)

By the Taylor expansion of Eq. 1 to the first order in the propagation direction z we arrive at a linear description of how the intensity changes between two image planes a small distance apart. This can be written as

$$\nabla[I_0(\mathbf{x}) \nabla \varphi(\mathbf{x})] = -\frac{2\pi}{\lambda} \frac{\partial}{\partial z} I_0(\mathbf{x}) \tag{2}$$

and is known as the transport of intensity equation [5, 8]. I_0 is the intensity at $D = 0$ and ∇ is the gradient operator in the image plane and is implemented as $\nabla = i2\pi \mathcal{F}^{-1}(f, g)\mathcal{F}$. Eq. 2 can be solved for the phase [9]:

$$\varphi(\mathbf{x}) = -\frac{2\pi}{\lambda} \nabla^{-2} \left(\nabla \cdot \left\{ \frac{1}{I_0(\mathbf{x})} \nabla \left[\nabla^{-2} \frac{\partial}{\partial z} I(\mathbf{x}) \right] \right\} \right) \tag{3}$$

Table 1. Theoretical values for the absorption coefficient and refractive index at 24 keV for the materials used in the phantom. These values were also used in the simulated data.

	μ (cm^{-1})	$2\pi\eta/\lambda$ $(\times 100 cm^{-1})$
Aluminium	4.650	11.4
Ethanol	0.135	4.00
Oil	0.101	4.36
PMMA	0.201	5.63
Polymer	0.108	5.00
Water	0.290	4.87

Due to the Taylor expansion, this expression is only valid for short propagation distances. Under this condition, it is possible to approximate the partial derivative in the z direction by a finite difference. This means that for this method, two images have to be recorded for each projection angle: one at $D \approx 0$ to obtain the absorption and one taken at a small distance away. The derivative is approximated by the difference between these two images.

The inverse Laplacian operator in Eq. 3 is implemented as $\nabla^{-2} = -\mathcal{F}^{-1}(f^2 + g^2)^{-1}\mathcal{F}$. This means that phase retrieval with the TIE requires 6 FFTs per projection angle. The main drawback of this method is the approximation of the partial derivative. It can be difficult to achieve sufficient signal to noise ratio in a difference between two images taken a small distance apart. Contrast can be improved by increasing the distance, but since the model is only valid for small distances, modelization errors will increase.

3.2. Contrast Transfer Function (CTF)

An alternative method can be derived if approximations are made regarding the object. If the complex exponentials in the transmittance function are Taylor expanded to the first order, Eq. 1 becomes [6]

$$\tilde{I}_D(\mathbf{f}) = \delta(\mathbf{f}) - 2\cos(\pi\lambda D \mathbf{f}^2)\tilde{B}(\mathbf{f}) + 2\sin(\pi\lambda D \mathbf{f}^2)\tilde{\varphi}(\mathbf{f}) \tag{4}$$

which is known as the contrast transfer function and is a linear approximation of how the Fourier transform of the intensity at distance D depends on the Fourier transforms of the amplitude and the phase of the transmitted wave. This can be shown to be valid for "weak" absorption and slowly varying phase [6]. Eq. 4 can be solved for the phase in a least squared error sense [10]

$$\tilde{\varphi}(\mathbf{f}) = \frac{1}{2\triangle} \left[C \sum_D \tilde{I}_D \sin(\pi\lambda D \mathbf{f}^2) - A \sum_D I_D \cos(\pi\lambda D \mathbf{f}^2) \right] \tag{5}$$

with $A = \sum_D \sin(\pi\lambda D \mathbf{f^2}) \cos(\pi\lambda D \mathbf{f^2})$, $B = \sum_D \sin^2(\pi\lambda D \mathbf{f}^2)$, $C = \sum_D \cos^2(\pi\lambda D \mathbf{f}^2)$ and $\triangle = BC - A^2$. Since the CTF has zero crossings, images at several distances are needed to solve Eq. 4. If N distances are used, calculation of the phase using Eq. 5 requires $N + 1$ FFTs. The main drawback of this method is that it is not valid for strongly absorbing objects, which is the case in many applications of interest, e.g. imaging of soft tissue in biological samples in the presence of bone.

3.3. Mixed approach

It can be shown that the TIE equation and CTF models do not approach the same solution, in the case of a strongly absorbing object, when $D \to 0$. By instead Taylor expanding the phase only in Eq. 1,

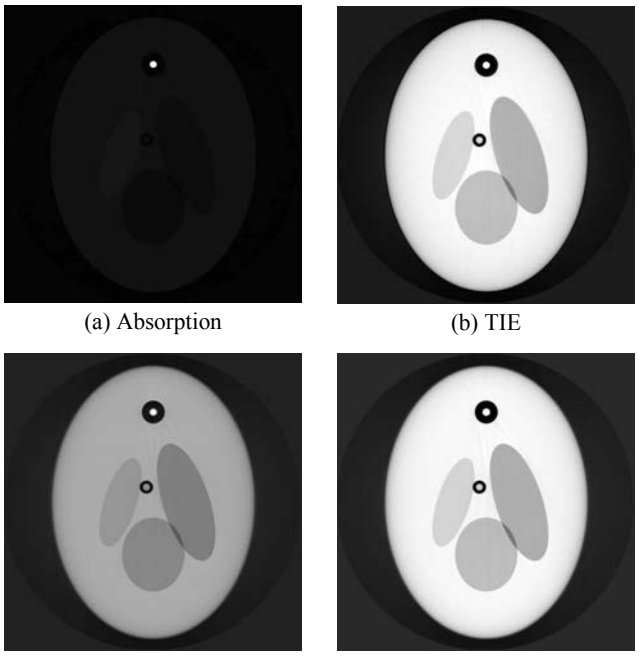

(a) Absorption (b) TIE

(c) CTF (d) Mixed

Fig. 3. Absorption and phase tomograms using the simulated data. Reconstruction was done using (a) the absorption radiographs (images simulated close to the detector) and output from the (b) TIE, (c) CTF and (d) mixed approach algorithms. The field of view is 15.4 mm.

we can approximate the recorded intensity as [7]

$$\begin{aligned} I_D(\mathbf{f}) &= I_D^{\varphi=0}(\mathbf{f}) + 2\sin(\pi\lambda D\mathbf{f}^2)\mathcal{F}\{I_0\varphi\}(\mathbf{f}) \\ &\quad + \cos(\pi\lambda D\mathbf{f}^2)\frac{\lambda D}{2\pi}\mathcal{F}\{\nabla(\nabla I_0\varphi)\}(\mathbf{f}) \end{aligned} \tag{6}$$

where $I_D^{\varphi=0}$ is the intensity at distance D if the phase of the object was zero. This can be either calculated exactly from $a(\mathbf{x}) = \sqrt{I_0(\mathbf{x})}$ or approximated by $\tilde{I}_0(\mathbf{f})$.

Eq. (6) is valid for slowly varying objects and approaches the TIE when $D \to 0$. It can be considered as an extension of the TIE valid for larger distances. Eq. 6 can be solved by considering the third term a perturbation term. A first estimate of $\varphi(\mathbf{x})$ is obtained by disregarding this term and subsequently improving the estimate iteratively. Different distances are taken into account by a linear least squares fitting of the phase to the perturbed data

$$\mathcal{F}\{I_0\varphi^{(n+1)}\}(\mathbf{f}) = \frac{\sum_D A_D(\mathbf{f})[\tilde{I}_D(\mathbf{f}) - \tilde{I}_D^{\varphi=0}(\mathbf{f}) - \Delta_D(\mathbf{f})]}{\sum_D A_D^2(\mathbf{f})} \tag{7}$$

where $\Delta_D(\mathbf{f}) = \cos(\pi\lambda D|\mathbf{f}|^2)\frac{\lambda D}{2\pi}\mathcal{F}\{\nabla(\varphi^{(n)}\nabla I_0)\}(\mathbf{f})$, $A_D(\mathbf{f}) = 2\sin(\pi\lambda D|\mathbf{f}|^2)$ and $\varphi^{(n)}(\mathbf{x})$ is the phase at iteration n with $\varphi^{(0)} = 0$. A smoothed version of $I_0(\mathbf{x})$ is used to adhere more closely to the slowly varying object condition. This is implemented using a standard Gaussian filter, applied in the Fourier domain.

Eq. 7 generally converges in 3-5 iterations. Since the first estimate requires N FFTs (with N typically 4) and the subsequent iterations require 2 FFTs each, between 10 and 14 FFTs are typically required to retrieve the phase.

Table 2. Simulated data: mean values and standard deviations of $2\pi\eta/\lambda$ ($\times 100cm^{-1}$) obtained from the central slices of the tomographic reconstructions.

	TIE	CTF	Mixed
Aluminium	9.28 ± 0.14	7.33 ± 0.11	9.50 ± 0.21
Ethanol	3.73 ± 0.05	3.63 ± 0.02	3.95 ± 0.02
Oil	4.03 ± 0.04	3.90 ± 0.02	4.32 ± 0.03
PMMA	5.10 ± 0.22	4.91 ± 0.11	5.52 ± 0.16
Polymer	4.68 ± 0.04	4.20 ± 0.05	4.93 ± 0.15
Water	4.55 ± 0.03	4.34 ± 0.02	4.84 ± 0.02

4. IMPLEMENTATION

4.1. Simulated data

Simulation of propagation based phase contrast imaging can be separated in two steps: calculating projections and simulating propagation. First, two projection data sets, one for the absorption and one for the phase shift, were generated by calculating analytical projections of an ellipsoid phantom based on the 3D Shepp-Logan phantom. The different regions in the simulated phantom were given the theoretical refractive indices of the materials used to construct the real phantom (table 1). The outer ring was removed and the areas of high absorption were surrounded by areas of zero absorption to closer resemble the qualitative behaviour of the constructed phantom. The projections, consisting of 2048×2048 pixels with a pixel size of 7.5 μm, were generated over 180 degrees using 1000 intervals. The center slice of the absorption and phase phantoms are shown in Fig. 2.

For each projection, the absorption and phase shift were combined to form a complex wave function. A convenient way to simulate propagation is to observe that a Fresnel diffraction pattern can also be described as convolution of the wave function with a propagator [10] . We calculated this in the Fourier domain, where the propagator becomes

$$P_D(\mathbf{x}) = \exp(-i\pi\lambda D\mathbf{f}^2) \tag{8}$$

The simulated intensity was then obtained by taking the squared modulus of the propagated wave. Finally, the intensities were interpolated to 512×512 pixels, which means that the diffraction patterns were simulated using 4 times oversampling and the final pixel size was $30\mu m$.

4.2. Constructed phantom

To evaluate the algorithms under experimental conditions, a phantom was constructed. Five channels were drilled in a 7.5 mm diameter PMMA cylinder and then filled with demineralized water, 96 % ethanol, oil, a length of 0.125 mm diameter aluminium wire and a mixture of polymer spheres, 0.1 and 0.2 mm diameter respectively. The phantom was then imaged using the ID19 micro-CT setup at the ESRF. Tomographic scans were acquired using 24 keV X-rays at four distances (0.012, 0.1, 0.3 and 0.99 m) and 1000 angular positions. A 2048x2048 CCD detector was used at a pixel size of $7.5\mu m$.

5. RESULTS

Both simulations and reconstructions were performed using GNU Octave software on the ESRF computing cluster and were run in a parallel fashion using the fact that each projection can be considered independent. This was implemented using Condor software.

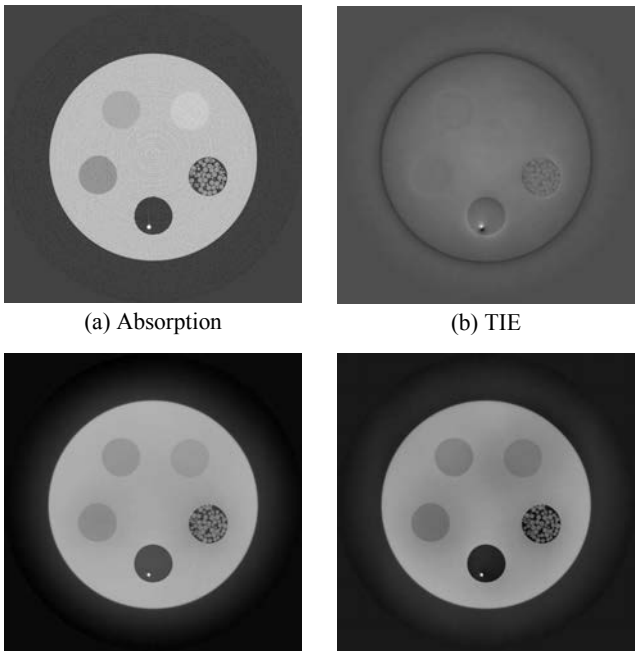

(a) Absorption (b) TIE

(c) CTF (d) Mixed

Fig. 4. Absorption and phase tomograms of the constructed phantom, consisting of a PMMA cylinder, demineralized water, 96% ethanol, oil, 0.125mm aluminium wire and polymer spheres, imaged at 24 keV. Reconstruction was done using (a) absorption radiographs (images taken close to the detector) and output from the (b) TIE (c) CTF and (d) mixed approach algorithms. The field of view is 15.4 mm.

5.1. Simulated data

Results using simulated data are presented in Fig. 3, which show that all three methods give qualitatively good reconstructions. Mean values and standard deviations were measured in the different areas (table 2). The mean errors compared to the theoretical values in table 1 are 10 % for the TIE, 16 % for the CTF and 3.8 % for the Mixed approach. Note that all the methods give underestimations of the refractive index, more so in areas with a higher absorption coefficient.

5.2. Constructed phantom

Examining the reconstructed slices (Fig. 4), the CTF and Mixed approach yield visually good reconstructions, while the TIE fails to reconstruct the cylinder properly. This is probably due to the difficulty of achieving enough SNR in the difference image. Measuring the means and standard deviations as before (table 3), we obtain mean errors of 42 % for the TIE, 17 % for the CTF and 5.9 % for the Mixed approach. Again we note that both the CTF and Mixed approach systematically underestimates the refractive index.

5.3. DISCUSSION AND CONCLUSION

Three methods for phase retrieval for propagation based imaging were evaluated. This was done using simulated data and experimental data acquired on a constructed phantom. The reconstructions were compared to theoretical values for the different materials used. Using the TIE on simulated data, a quantitative reconstruction of the refractive index was obtained, with an average error of 10 %. On experimental data however, we failed to achieve a qualitative result. Using the CTF, qualitative reconstructions were obtained both on simulated and experimental data, with consistently underestimated values. Using the Mixed approach reconstructions with close correspondence to expected values were obtained, both for simulated and experimental data, with an average error of 3.8 % and 5.9 % respectively.

The main contribution in the work is the framework for evaluating phase retrieval algorithms. The implemented tests are intended as a platform for evaluation of existing as well as new phase retrieval algorithms. They could be used to investigate noise sensitivity or finding optimal experimental conditions for different phase retrieval algorithms.

Table 3. Constructed phantom: mean values and standard deviations of $\pi\eta/\lambda$ ($\times 1 \quad cm^{-1}$) obtained from the central slices of the tomographic reconstructions.

	TIE	CTF	Mixed
Aluminium	22.2 ± 8.23	7.09 ± 0.16	9.24 ± 0.19
Ethanol	$6.\ 9 \pm 0.04$	3.60 ± 0.05	3.98 ± 0.08
Oil	5.79 ± 0.0	$4.\ 5 \pm\ .\ 6$	$4.33 \pm\ .\ 3$
PMMA	5.13 ± 1.94	$5.\quad \pm 0.\ 3$	$5.56 \pm 0.\ 3$
Polymer	6.85 ± 0.03	3.48 ± 0.15	$4.41 \pm 0.\ 3$
Water	5.83 ± 0.08	4.27 ± 0.07	4.75 ± 0.08

6. REFERENCES

[1] A. Momose and J. Fukuda, "Phase-contrast radiographs of nonstained rat cerebellar specimen," *Med. Phys.*, vol. 22, pp. 375–379, 1994.

[2] P. Cloetens, W. Ludwig, E. Boller, L. Helfen, L. Salvo, R. Mache, and M. Schlenker, "Quantitative phase contrast tomography using coherent synchrotron radiation," *Proceedings of the SPIE*, vol. 4503, pp. 82–91, 2002.

[3] P. Cloetens, W. Ludwig, J. Baruchel, D. Van Dyck, J. Van Landuyt, J. P. Guigay, and M. Schlenker, "Holotomography: Quantitative phase tomography with micrometer resolution using hard synchrotron radiation x rays," *Appl. Phys. Lett.*, vol. 75, pp. 2912–2914, 1999.

[4] A. Barty, K. A. Nugent, D. Paganin, and A. Roberts, "Quantitative optical phase microscopy," *Opt. Lett.*, vol. 23, pp. 817–819, 1998.

[5] M. R. Teague, "Irradiance moments: their propagation and use for unique retrieval of phase," *J. Opt. Soc. Am.*, vol. 72, pp. 1199–1209, 1982.

[6] J. P. Guigay, "Fourier transform analysis of Fresnel diffraction patterns and in-line holograms," *Optik*, vol. 46, pp. 121–125, 1977.

[7] J.-P. Guigay, M. Langer, and P. Cloetens, "A mixed contrast transfer and transport of intensity approach for phase retrieval in the Fresnel region," In preparation.

[8] K.A. Nugent, T.E. Gureyev, D.F. Cookson, D. Paganin, and Z. Barnea, "Quantitative phase imaging using hard x rays," *Phys. Rev. Lett.*, vol. 77, pp. 2961–2964, 1996.

[9] D. M. Paganin, *Coherent X-Ray Optics*, Oxford University Press, 2006.

[10] S. Zabler, P. Cloetens, J.-P. Guigay, J. Baruchel, and M. Schlenker, "Optimization of phase contrast imaging using hard x rays," *Rev. Sci. Instrum.*, vol. 76, pp. 1–7, 2005.